Nanoscale Advances

ROYAL SOCIETY OF CHEMISTRY

PAPER

View Article Online
View Journal | View Issue



Cite this: *Nanoscale Adv.*, 2020, **2**, 808

# Charge transfer between lead halide perovskite nanocrystals and single-walled carbon nanotubes†

Parul Bansal,[ab] Xiangtong Zhang,[b] Hua Wang,[b] Prasenjit Kar *[a] and William W. Yu *[b]

A charge transfer study between lead halide-based perovskite nanocrystals and single-walled carbon nanotubes (PNC@CNT nanocomposite) was performed. Solution-processed $MAPbX_3$ PNCs displayed very bright luminescence, but it quenched in the presence of CNTs. This was attributed to the electron transfer from PNCs to CNTs. The detailed changes in fluorescence lifetime were investigated through time-correlated single-photon counting (TCSPC), which suggested mixed static and dynamic quenching along with a decrease in the lifetime. Morphological changes were investigated *via* transmission electron microscopy (TEM) and attributed to the incorporation of PNCs on long CNTs. Also, the PNC@CNT nanocomposite was explored for photoinduced current response, which indicated an ~3 fold increase in photoconductivity under light illumination (with a 1 mV bias). This electron transfer study between PNCs and CNTs contributes to the exploration of charge dynamics.

Received 7th December 2019
Accepted 2nd January 2020

DOI: 10.1039/c9na00766k

rsc.li/nanoscale-advances



## 1. Introduction

Metal halide perovskites[1] have emerged among the superior materials for optoelectronic devices[2–4] including light-emitting diodes,[4] solar cells,[5,6] photodetectors, lasers, and in light harvesting.[2,3,8–12] The efficacy of these applications relies on good absorption characteristics, easy charge carrier formation and transport in these materials.[2,13–15] Besides, the low-cost solution synthesis of these perovskite nanocrystals (PNCs) results in intense fluorescence and nearly unity quantum yield.[2,16–21] On the other hand, the strong confinement of carbon nanotubes (CNTs) to one dimension has also attracted the attention of the scientific community in the areas of charge transport, field emission, gas storage, photodetectors and other photovoltaic applications.[22,23] Advancement in this research field has been probed through various photo-responsive CNT-based nanocomposites with organic fluorophores and inorganic moieties including conventional quantum dots (*e.g.*, CdSe/ZnS).[24–28] The mechanistic investigation of CNTs and quantum dots revealed that the excited states of fluorescent quantum dots donate either excited electrons or holes to CNTs, which leads to the quenching of the photoluminescence.[25]

PNCs have size-dependent properties[7,17] because of the quantum confinement effect, whereas CNTs have high electron transfer properties because of their nanoscale size, large surface area and direct path for charge transport.[29–31] The formation of nanocomposites by combining the properties of both materials will lead to new avenues of opportunities in the field of nanotechnology. The photo-excited electron can be transferred from electron donor PNCs to electron acceptor CNTs. Earlier investigations on electron migration through static fluorescence quenching have been performed by Nair *et al.* using $FAPbBr_3$ and fullerene $C_{60}$.[32] Kuang and coworkers studied the improvements in the charge transfer and light-harvesting properties of mixed cesium lead halide PNCs and CNTs.[33] Chen and colleagues recently reported graphene sandwich stable PNC light-emissive ultrasensitive and ultrafast broadband phototransistors.[34]

Herein, we report a detailed electron transfer study using single-walled CNTs and methylammonium lead halide PNCs. The preference of single-walled CNTs over $C_{60}$ fullerene is due to their superior electron transfer properties. Also, we have investigated the steady-state photoluminescence and the corresponding time-resolved lifetime, through which we have found a mixture of static and dynamic quenching (Fig. 1). The

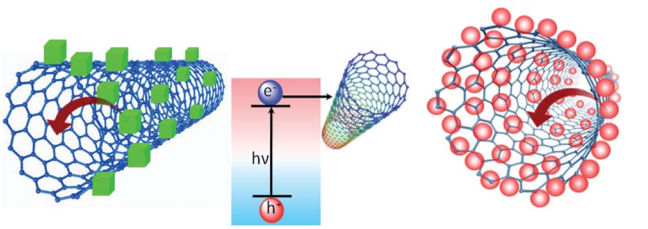


Fig. 1 Schematic representation of electron transfer from $MAPbX_3$ to a single-walled carbon nanotube.

[a]*Department of Chemistry, Indian Institute of Technology Roorkee, Uttarakhand 247667, India. E-mail: kar.prasen@gmail.com; prkarfcy@iitr.ac.in*

[b]*Department of Chemistry and Physics, Louisiana State University Shreveport, Louisiana 71115, USA. E-mail: wyu6000@gmail.com*

† Electronic supplementary information (ESI) available. See DOI: 10.1039/c9na00766k

methods of preparation of $MAPbBr_3$, $MAPbI_3$ and CNT solutions are detailed in the ESI.†

The absorption spectra of blue luminescent $MAPbBr_3$ and red luminescent $MAPbI_3$ are shown in Fig. 2a, and images of $MAPbI_3$ PNCs in daylight and UV light are presented in Fig. 2b and c. Images of green and blue luminescent $MAPbBr_3$ PNCs in the presence of increasing concentrations of CNT are shown in Fig. S1.† XRD patterns of synthesized perovskite nanocrystals are shown in Fig. S2† for blue luminescent $MAPbBr_3$ and red luminescent $MAPbI_3$, confirming the presence of the cubic and tetragonal phases in $MAPbBr_3$ and $MAPbI_3$ PNC.[17] Absorption peaks of $MAPbBr_3$ solution were observed at 462 nm and at 563 and 604 nm for $MAPbI_3$ in the presence of CNTs. $MAPbX_3$ PNCs are highly fluorescent and their optical properties can be easily modified by size variation. The addition of CNTs to PNC solution leads to the adhering of quantum dots to the walls of CNTs because of van der Waals interactions. In our case, we sonicated the CNT solution for a longer time to separate the CNT bundles and increase the surface area of CNTs so that electron transfer would take place more efficiently. Pristine CNTs (not functionalized) were used, and the presence of oleic acid and oleylamine helped the adhesion of PNCs to the walls of the CNTs. To monitor the effect of solvent (*i.e.* $CHCl_3$), we performed the emission studies in the presence of $CHCl_3$ (without the addition of CNT) and with respect to time as shown in Fig. S3,† indicating the negligible effect of the solvent, which confirmed that the quenching is due to the adhesion of perovskite nanocrystals to CNTs.

As shown in Fig. 3a–c, there was almost 100% fluorescence quenching of blue, green and red luminescent PNCs with CNTs, which is clear evidence that the electron transfer takes place from the electron donor PNCs to the acceptor CNT bundles. The quenching experiment was performed with the sequential addition of CNT solution (0.01% w/v in chloroform) from 10 μL to 300 μL. We observed blue shifts in all PNC peaks as compared to previous reports[17] due to the dilution of samples before quenching studies. In Fig. 3a–c, the emission peaks of the blue luminescent $MAPbBr_3$, green luminescent $MAPbBr_3$ and red luminescent $MAPbI_3$ (without CNTs) were observed at 443 nm, 510 nm and 596 nm, respectively.

We observed almost 100% quenching with the addition of 300 μL of CNT solution for all three PNCs. Apart from the quenching of the emission peaks, we also observed blue shifts in the spectra (initially) on increasing the amount of CNT (predominantly for blue luminescent $MAPbBr_3$ PNCs). The rate of PL quenching was nonlinear as shown in Fig. 3d–f. A possible reason for these PNC@CNT nanocomposites to give nonlinear Stern–Volmer plots is the presence of both static and dynamic quenching.[35] Fig. 3d–f shows curves along with exponential equations and rate constants for blue, green and red luminescent PNCs, respectively.

The most efficient way to determine whether quenching is static, dynamic or both is through PL decay lifetime measurements. If the lifetime values remain unchanged in the presence of CNTs, it might be due to static quenching, as previously reported with $FAPbBr_3$ and fullerene.[28] However, in the case of $MAPbX_3$ PNCs there was a decrease in the lifetime of PNCs with increasing the amount of CNTs, which was attributed to the presence of static and dynamic quenching as shown in Fig. 3g–i. The average lifetimes along with the details of parameters for blue, red and green luminescent PNCs in the presence of CNT solution are listed in Table 1. The average lifetime was calculated by the following formula:

$$\tau_{avg} = (A_1\tau_1^2 + A_2\tau_2^2 + A_3\tau_3^2)/(A_1\tau_1 + A_2\tau_2 + A_3\tau_3)$$

where $A_1$, $A_2$ and $A_3$ are weighing parameters, $\tau_1$, $\tau_2$ and $\tau_3$ are the corresponding lifetimes and $\tau_{avg}$ is the average lifetime.

The X-ray diffraction (XRD) pattern of $MAPbBr_3$@CNT is provided in Fig. S4,† showing the presence of perovskite peaks. TEM images of blue, green and red luminescent $MAPbX_3$ PNCs are given in Fig. S5.† From Fig. S5,† the tunable morphology is directly evidenced by the TEM images, where the morphology changes from quantum dots to nanoplates to quantum dots by shifting from blue-green-red luminescent $MAPbX_3$ PNCs, which leads to adhesion to CNTs as shown in Fig. 4. These interactions are due to the electron migration or transfer from electron donor halide perovskites to electron acceptor CNTs. TEM images of PNC@CNT nanocomposites provide direct evidence of PNCs adhering to CNTs as shown in Fig. 4. The typical Fourier transform-infrared spectroscopy (FT-IR) vibration modes are presented in Fig. S6.† XPS analysis of green luminescent $MAPbBr_3$ in the presence of CNT confirms the presence of the elemental composition of PNC with the main peaks of Pb 4f, C 1s, N 1s and Br 3d in narrow scans as shown in Fig. S7.†

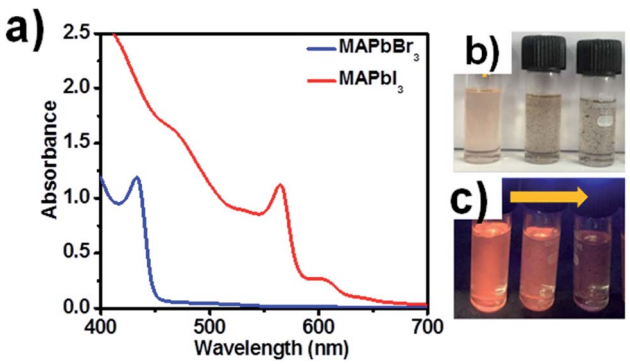


Fig. 2 (a) Absorption spectra of $MAPbBr_3$ and $MAPbI_3$ PNCs in the presence of CNTs. (b) Daylight images of $MAPbI_3$ solution with increasing concentration of CNTs (from left to right). (c) $MAPbI_3$ solution with increasing concentration of CNTs (from left to right) under UV light.

## 2. Photoresponse study

A prototype device was fabricated to investigate the conductive properties of the PNC@CNT nanocomposite. A schematic illustration is provided in Fig. 5 for measuring the photoconductivity. The device was made by two silver electrodes separated by 0.5 mm on a silica substrate and drop-casting the concentrated $MAPbI_3$@CNT nanocomposite sample to connect the two electrodes. The photoinduced current was measured on

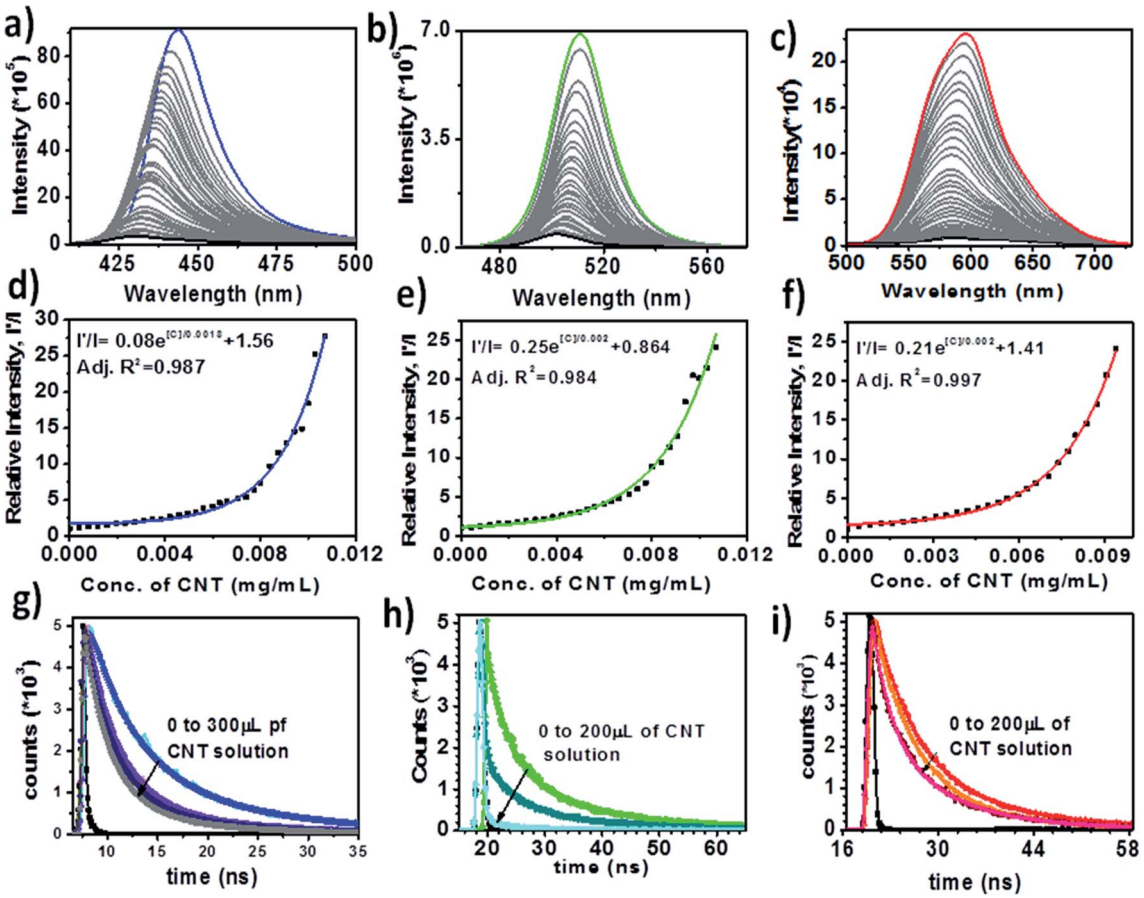


Fig. 3 Photoluminescence (PL) quenching of (a) blue luminescent $MAPbBr_3$, (b) green luminescent $MAPbBr_3$, and (c) red luminescent $MAPbI_3$ PNCs with CNTs. (d) Relative PL intensity changes with CNT concentration on the quenching of (d) blue, (e) green, and (f) red luminescent PNCs. TCSPC measurements of (g) blue, (h) green and (i) red luminescent PNCs on the addition of CNTs. The CNTs were added in the form of 0.01% w/v solution.

a Keithley 2612B source meter while irradiating the sample with a daylight lamp having a brightness of 1200 lumens. Fig. 5a shows the current–voltage curve of the nanocomposite in the dark and in the presence of light, displaying excellent ohmic responses. The resistance in the presence of light was 14.2 Ω, whereas in the dark it was 15.37 Ω, which confirms that irradiation in light leads to an increase in current (Fig. 5a). Photoinduced charge was generated in this device system upon irradiation with light.[21] It was found that the photoconductivity increased ~3 fold under light illumination at 1 mV voltage (Fig. 5b) and the photocurrent was basically constant over time as shown in Fig. 5b, indicating the good stability of the nanocomposite over a number of cycles. It has been confirmed that the presence of CNT alone does not lead to the change in current under light irradiation.[36,37] As such, the increase in the current (Fig. 5a and b) was due to the presence of PNCs and that

Table 1 TCSPC details of PNC solutions in the presence of CNT

| Sample | CNT volume (µL) | $A_1$ | $A_2$ | $A_3$ | $\tau_1$ (ns) | $\tau_2$ (ns) | $\tau_3$ (ns) | $\tau_{avg}$ (ns) |
|---|---|---|---|---|---|---|---|---|
| Blue $MAPbBr_3$ | 0 | 32.24 | 53.35 | 14.40 | 4.23 | 10.53 | 60.08 | 37.40 |
| | 100 | 48.31 | 41.89 | 9.80 | 2.82 | 8.14 | 53.82 | 31.40 |
| | 200 | 34.87 | 9.84 | 55.29 | 8.93 | 55.41 | 2.88 | 32.92 |
| | 300 | 37.35 | 9.44 | 53.22 | 7.69 | 46.58 | 2.45 | 26.88 |
| Green $MAPbBr_3$ | 0 | 41.95 | 27.51 | 30.54 | 9.05 | 0.12 | 32.63 | 26 |
| | 100 | 3.76 | 3.96 | 92.27 | 6.12 | 24.96 | 0.044 | 20 |
| | 200 | 9.04 | 12.93 | 78.03 | 2.75 | 17.81 | 0.25 | 15.19 |
| Red $MAPbI_3$ | 0 | 37.60 | 54.26 | 8.14 | 5.63 | 12.03 | 52.30 | 24.26 |
| | 100 | 47.62 | 47.56 | 4.86 | 5.41 | 10.26 | 49.35 | 18.51 |
| | 200 | 22.10 | 67.51 | 10.39 | 2.56 | 9.03 | 31.68 | 16 |

 

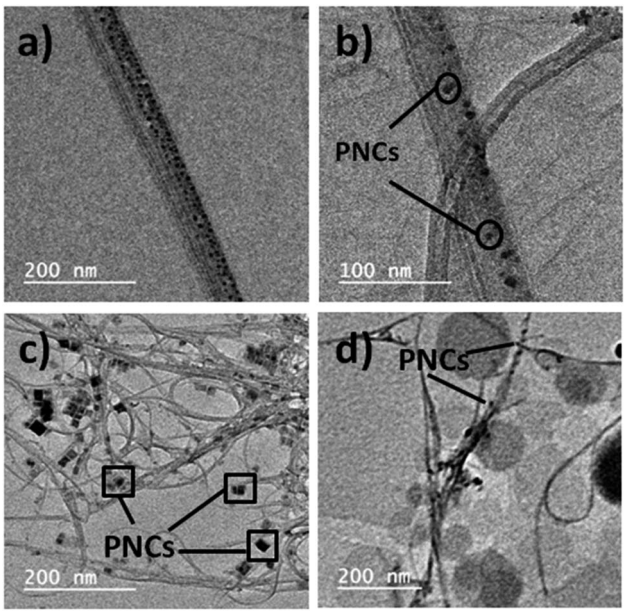


Fig. 4 TEM images of (a), (b) blue, (c) green and (d) red luminescent PNCs in the presence of CNTs.

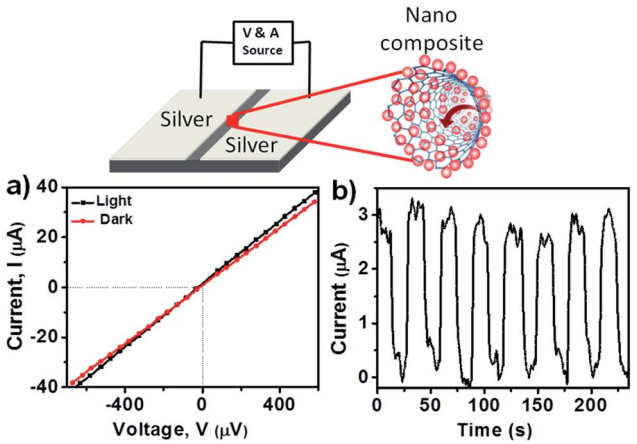


Fig. 5 Schematic illustration of the fabricated device (top); (a) the *I*–*V* curve for $MAPbI_3$@CNT in the presence and absence of light and (b) the corresponding *I*–*t* curve for $MAPbI_3$@CNT.

led to the charge transfer between CNTs and PNCs and completed the circuit. For multiple current cycle investigations, the light was turned on and off with a 15 s interval.

Photocurrent ($I_{ph}$) was evaluated by $I_{ph} = |I_l - I_d|$ where $I_d$ is the current in the dark and $I_l$ is the current under illumination. As shown in Fig. 5b, the PNC@CNT nanocomposite exhibited a photocurrent which led to a difference in current under light irradiation. The device exhibited a photocurrent of 2.92 μA because of the adhesion of PNCs on CNTs through van der Waals interactions. Applied bias led to the generation of charge carriers that migrated from the electron donor PNCs to electron acceptor CNTs, leading to the enhancement of the current. These results indicate that charge transfer between PNCs and CNTs produced a noticeable photocurrent, which paves the way towards new optoelectronic and nanosensor-based applications.

## 3. Conclusions

In summary, we studied the charge transfer behaviour between lead halide based perovskites and carbon nanotubes. Fluorescence quenching and lifetime studies revealed the presence of static as well as dynamic quenching. TEM morphological studies and PL quenching also indicated significant interaction enhancement between PNCs and CNTs. Photoconductive perovskite nanocomposites have opened new avenues for solar cells, sensor-based nanodevices and light-driven optoelectronics.

## Conflicts of interest

There are no conflicts of interest to declare.

## Acknowledgements

This work was supported by Indian Institute of Technology Roorkee and Louisiana State University in Shreveport, LA, USA. P. K. acknowledges the Council of Scientific & Industrial Research (CSIR (01(2990)/19/EMR-II)), New Delhi, India. Authors acknowledge Institute Instrumentation Centre (IIC), IIT Roorkee for instrument facility. P. B. acknowledges J. William Fulbright Foreign Scholarships Board (FFSB), United States-India Educational Foundation (USIEF) and Institute of International Education (IIE) for Fulbright-Nehru Doctoral Program.

## References

1 L. C. Schmidt, A. Pertegás, S. González-Carrero, O. Malinkiewicz, S. Agouram, G. Mínguez Espallargas, H. J. Bolink, R. E. Galian and J. Pérez-Prieto, Non Template Synthesis of $MAPbBr_3$ Perovskite Nanoparticles, *J. Am. Chem. Soc.*, 2014, **136**, 850–853.

2 H. Huang, L. Polavarapu, J. A. Sichert, A. S. Susha, A. S. Urban and A. L. Rogach, Colloidal Lead Halide Perovskite Nanocrystals: Synthesis, Optical Properties and Applications, *NPG Asia Mater.*, 2016, **8**, e328.

3 Y. Zhao and K. Zhu, Organic and Inorganic Hybrid Lead Halide Perovskites for Optoelectronic and Electronic Applications, *Chem. Soc. Rev.*, 2016, **45**, 655.

4 M. Lu, J. Guo, P. Lu, L. Zhang, Y. Zhang, Q. Dai, Y. Hu, V. L. Colvin and W. W. Yu, Ammonium-Thiocyanate-Passivated $CsPbI_3$ Perovskite Nanocrystals for Efficient Red Light-Emitting Diodes, *J. Phys. Chem. C*, 2019, **123**, 22787–22792.

5 A. Kojima, K. Teshima, Y. Shirai and T. Miyasaka, Organometal Halide Perovskites as Visible-Light Sensitizers for Photovoltaic Cells, *J. Am. Chem. Soc.*, 2009, **131**, 6050–6051.

6 (*a*) M. M. Lee, J. Teuscher, T. Miyasaka, T. N. Murakami and H. J. Snaith, Efficient Hybrid Solar Cells Based on Meso-

superstructured Organometal Halide Perovskites, *Science*, 2012, **338**, 643–647; (*b*) M. F. Aygüler, M. D. Weber, B. M. D. Puscher, D. D. Medina, P. Docampo and R. D. Costa, Light Emitting Electrochemical Cells Based on Hybrid Lead Halide Perovskite Nanoparticles, *J. Phys. Chem. C*, 2015, **119**, 12047–12054.

7 L. Protesescu, S. Yakunin, M. I. Bodnarchuk, F. Krieg, R. Caputo, C. H. Hendon, R. X. Yang, A. Walsh and M. V. Kovalenko, Nanocrystals of Cesium Lead Halide Perovskites ($CsPbX_3$, X = Cl, Br and I): Novel Optoelectronic Materials Showing Bright Emission with Wide Color Gamut, *Nano Lett.*, 2015, **15**, 3692–3696.

8 (*a*) C. Muthu and V. C. Nair, $CH_3NH_3PbBr_3$ Perovskite Nanocrystals as Efficient Light-Harvesting Antenna for Fluorescence Resonance Energy Transfer, *Chem. - Asian J.*, 2017, **12**, 988–995; (*b*) P. Bansal and P. Kar, Probing the Energy Transfer Process by Controlling the Morphology of $CH_3NH_3PbBr_3$ Nanocrystals with Rhodamine B Dye, *J. Lumin.*, 2019, **215**, 116609.

9 J. Zhang, C. Wang, X. Shen, M. Lu, J. Guo, X. Bai, Y. Zhang and W. W. Yu, Perovskite Light Emitting Diodes for Uniform Eight-Segment Displays, *Appl. Phys. Lett.*, 2019, **115**, 193104.

10 P. Lu, M. Lu, H. Wang, N. Sui, Z. Shi, W. W. Yu and Y. Zhang, Metal Halide Perovskite Nanocrystals and Their Applications on Optoelectronic Devices, *InfoMat*, 2019, **1**, 1–29.

11 M. Lu, H. Wu, X. Zhang, H. Wang, Y. Hu, V. L. Colvin, Y. Zhang and W. W. Yu, Highly Flexible $CsPbI_3$ Perovskite Nanocrystal Light-Emitting Diodes, *ChemNanoMat*, 2019, **5**, 313–317.

12 H. Wu, Y. Zhang, M. Lu, X. Zhang, C. Sun, T. Zhang, V. L. Colvin and W. W. Yu, Surface Ligand Modification of Cesium Lead Bromide Nanocrystals for Improved Light-Emitting Performance, *Nanoscale*, 2018, **10**, 4173–4178.

13 G. Xing, N. Mathews, S. Sun, S. S. Lim, Y. M. Lam, M. Grätzel, S. Mhaisalkar and T. C. Sum, Long-Range Balanced Electron and Hole-transport Lengths in Organic-Inorganic $CH_3NH_3PbI_3$, *Science*, 2013, **342**, 344–347.

14 A. M. Ontoria, I. Zimmermann, I. Garcia-Benito, P. Gratia, C. Roldän-Carmona, S. Aghazada, M. Grätzel, M. K. Nazeerudin and N. Martin, Benzotrithiophene-Based Hole-Transporting Materials for 18.2% Perovskite Solar Cells, *Angew. Chem., Int. Ed.*, 2016, **55**, 6270–6274.

15 (*a*) S. D. Stranks, G. E. Eperon, G. Grancini, C. Menelaou, M. J. P. Alcocer, T. Leijtens, L. M. Herz, A. Petrozza and H. J. Snaith, Electron-Hole Diffusion Lengths Exceeding 1 Micrometer in an Organometal Trihalide Perovskite Absorber, *Science*, 2013, **342**, 341–343; (*b*) S. D. Stranks and H. J. Snaith, Metal Halide Perovskites for Photovoltaic and Light-emitting Devices, *Nat. Nanotechnol.*, 2015, **10**, 391–402.

16 H. C. Wang, S. Y. Lin, A. C. Tang, B. P. Singh, H. C. Tong, C. Y. Chen, Y. C. Lee, T. L. Tsai and R. S. Liu, Mesoporous Silica Particles Integrated with All-Inorganic $CsPbBr_3$ Perovskite Quantum-Dot Nanocomposites (MP-PQDs) with High Stability and Wide Color Gamut used for Backlight Display, *Angew. Chem., Int. Ed.*, 2016, **55**, 7924–7929.

17 P. Bansal, Y. Khan and P. Kar, High Luminescence Color Gradient by Physical Mixing of two Perovskite Nanocrystals, *New J. Chem.*, 2019, **43**, 4116–4122.

18 P. Bansal, Y. Khan, G. K. Nim and P. Kar, Surface Modulation of Solution Processed Organolead Halide Perovskite Quantum dots to Large Nanocrystals Integrated with Silica Gel G, *Chem. Commun.*, 2018, **54**, 3508–3511.

19 P. Bansal and P. Kar, Ultralong Micro-Belts of Luminescent Lead Halide based Perovskites, *Chem. Commun.*, 2019, **55**, 6543–6546.

20 D. Zhang, S. W. Eaton, Y. Yu, L. Dou and P. Yang, Solution-Phase Synthesis of Cesium Lead Halide Perovskite Nanowires, *J. Am. Chem. Soc.*, 2015, **137**, 9230–9233.

21 H. Lin, C. Zhou, M. Chaaban, L.-J. Xu, Y. Zhou, J. Neu, M. Worku, E. Berkwits, Q. He, S. Lee, X. Lin, T. Siegrist, M.-H. Du and B. Ma, Bulk Assembly of Zero-Dimensional Organic Lead Bromide Hybrid with Efficient Blue Emission, *ACS Mater. Lett.*, 2019, **1**, 594–598.

22 A. Javey, J. Guo, Q. Wang, M. Lundstorm and H. J. Dai, Ballistic Carbon Nanotube Field-Effect Transistors, *Nature*, 2003, **424**, 654–657.

23 D. Shahrjerdi, A. D. Franklin, S. Oida, J. A. Ott, G. S. Tulevski and W. Haensch, High Performance Air-Stable n-Type Carbon Nanotube Transistors with Erbium Contacts, *ACS Nano*, 2013, **7**, 8303–8308.

24 L. Wang, J. Han, Y. Zhu, R. Zhou, C. Jaye, H. Liu, Z.-Q. Li, G. T. Taylor, D. A. Fischer, J. Appenzeller and S. S. Wong, Probing the Dependence of Electron Transfer on Size and Coverage in Carbon Nanotube-Quantum Dot Heterostructures, *J. Phys. Chem. C*, 2015, **119**, 26327–26338.

25 J. E. Weaver, M. R. Dasari, A. Datar, S. Talapatra and P. Kohli, Investigating Photoinduced Charge Transfer in Carbon Nanotube-Perylene-Quantum Dot Hybrid Nanocomposites, *ACS Nano*, 2010, **4**, 6883–6893.

26 W. Feng, C. Qin, Y. Shen, Y. Li, W. Luo, A. Haoran and Y. Feng, A Layer-Nanostructured Assembly of PbS Quantum Dot/Multiwalled Carbon Nanotube for a High Performance Photoswitch, *Sci. Rep.*, 2013, **4**, 3777.

27 M. Olek, T. Büsgen, M. Hilgendorff and M. Giersig, Quantum Dot Modified Multiwall Carbon Nanotubes, *J. Phys. Chem. B*, 2006, **110**, 12901–12904.

28 A. D. Franklin and Z. Chen, Length Scaling of Carbon Nanotube Transistors, *Nat. Nanotechnol.*, 2010, **5**, 858–862.

29 G. Yu, J. C. Hummelen, F. Wudl and A. J. Heeger, Polymer Photovoltaic Cells-Enhanced Efficiencies *via* a Network of Internal Donor-Acceptor Heterojunctions, *Science*, 1995, **270**, 1789–1791.

30 S. Iijima, Helical Microtubules of Graphitic Carbon, *Nature*, 1991, **354**, 56–58.

31 J. A. Misewich, R. Martel, P. Avouris, J. C. Tsang, S. Heinz and J. Tersoff, Electrically Induced Optical Emission from a Carbon Nanotube FET, *Science*, 2003, **300**, 783.

32 V. C. Nair, C. Muthu, A. L. Rogach, R. Kohara and V. Biju, Channeling Exciton Migration into Electron Transfer in Formamidinium Lead Bromide Perovskite Nanocrystal/Fullerene Composites, *Angew. Chem., Int. Ed.*, 2017, **56**, 1214–1218.

 

33 M.-Z. Yang, Y.-F. Xu, J.-F. Liao, X.-D. Wang, H.-Y. Chen and D.-B. Kuang, Constructing $CsPbBr_xI_{3-x}$ Nanocrystals/Carbon Nanotube Composites with Improved Charge Transfer and Light Harvesting for Enhanced Photoelectrochemical Activity, *J. Mater. Chem. A*, 2019, **7**, 5409–5415.

34 K. P. Bera, G. Haider, Y.-T. Huang, P. K. Roy, C. R. P. Inbaraj, Y.-M. Liao, H.-I. Lin, C.-H. Lu, C. Shen, W. Y. Shih, W.-H. Shih and Y.-F. Chen, Graphene Sandwich Stable Perovskite Quantum dot Light Emissive Ultrasensitive and Ultrafast Broadband Vertical Phototransistors, *ACS Nano*, 2019, **13**, 12540–12552.

35 J. Liu, Y. Zhong, P. Lu, Y. Hong, J. W. Y. Lam, M. Faisal, Y. Yu, K. S. Wong and B. Z. Tang, A Superamplification Effect in the Detection of Explosives by a Fluorescent Hyberbranched Poly(silylenephenylene) with Aggregation-Enhanced Emission Characteristics, *Polym. Chem.*, 2010, **1**, 426–429.

36 X. L. Li, Y. Jia and A. Y. Gao, Tailored Single-Walled Carbon Nanotube CdS Nanoparticle Hybrids for Tunable Optoelectronic Devices, *ACS Nano*, 2009, **4**, 506–512.

37 R. Robel, B. A. Bunker and P. V. Kamat, Single-Walled Carbon Nanotube CdS Nanocomposites as Light Harvesting Assemblies Photoinduced Charge Transfer Interactions, *Adv. Mater.*, 2005, **17**, 2458–2463.